Ligand exchange used as double-edged sword for the removal of ammonia and dyes from wastewater

Marwa El-Ghobashy (marwa_elghobashy@science.tanta.edu.eg)
Tanta University Faculty of Science

Mohamed Khamis
Tanta University Faculty of Science

Abeer Elsherbiny
Tanta University Faculty of Science

Ibrahim Salem
Tanta University Faculty of Science

Research Article

Keywords: Ammonia, Amberlite IR-120, Complexation, R-Cu(II)-amine composite, Dyes, Removal

Posted Date: July 5th, 2022

DOI: https://doi.org/10.21203/rs.3.rs-1720551/v1

Ligand exchange used as double-edged sword for the removal of ammonia and dyes from wastewater

Marwa A. El-Ghobashy, Mohamed M. Khamis, Abeer S. Elsherbiny, Ibrahim A. Salem*
Chemistry Department, Faculty of Science, Tanta University, Tanta 31527, Egypt

Abstract

Cationic ligand exchange is one of the most predominant mechanisms for the removal of ammonia from wastewater through complex formation. The complexation technique occurs between the metal ions loaded on the surface of Amberlite IR-120 (R-H) and ammonia which is present in medium. Cu(II)-loaded Amberlite IR-120 (R-Cu^{2+}) was prepared and described using FT-IR, TGA, XRD, SEM, EDX techniques. The prepared R-Cu^{2+} was applied for elimination of ammonia from aqueous solution. Different cations such as Co^{2+}, Ni^{2+} were loaded onto Amberlite IR-120 to study the impact of counter cation on the removal efficiency of ammonia. The ammonia removal percentage followed the order; R-Cu^{2+} > R-Ni^{2+} > R-Co^{2+}. The removal of ammonia using R-Cu^{2+} obeyed Freundlich isotherm model. Thermodynamic parameters characteristics of the adsorption of ammonia onto R-Cu^{2+} were determined. The time-adsorption data were followed the pseudo-second-order and intraparticle diffusion models. Moreover, the resulting product (R-Cu(II)-amine composite) from the adsorption process exhibited high catalytic activity and could be applicable as low cost catalyst for enhancement the elimination of dyes from wastewater.

Keywords: Ammonia, Amberlite IR-120, Complexation, R-Cu(II)-amine composite, Dyes, Removal

……

*Corresponding Author : marwa_elghobashy@science.tanta.edu.eg (M. A. El-Ghobashy)

1. Introduction

Water is the most indispensable thing for the life on the earth. water contamination is one of the most serious issues facing humans and living organisms over the worldwide due to agricultural activities, industrialization and rapid-growing global population (Elkady, Salama et al. 2020). Ammonia nitrogen (NH_3-N) plays an essential role in marine life, it represents a nutrient for plant growth. However, it is the primary pollutant in wastewater, it results from municipal sewage, industrial wastewater and agricultural sources or from the decomposition of organic nitrogen compounds which discharged into water streams (Zhu, Chen et al. 2019). Fertilizers industry, manufacturing of many industrial products such as fibers, explosives, plastics, rubber, pulp, paper, chemicals and pharmaceuticals are considered the major source of ammonia contaminated water (Karri, Sahu et al. 2018).

Large amount of contaminated water that contains high concentrations of NH_3-N leak into the surrounding water resources. As a result, serious environmental problems were caused such as the eutrophication of surface water due to algae growth that leads to reduce of dissolved oxygen in water, and toxicity to fish and aquatic life (Adam, Othman et al. 2019, Zhu, Chen et al. 2019).

According to the World Health Organization (WHO) and the U.S. environmental protection agency (EPA), the level of NH_3-N in surface water more than 10 mg N L^{-1} is more dangerous to human health and other aquatic organisms' life (Liu, Chen et al. 2018). However, the maximum concentration of NH_3-N in drinking water and in natural water should be 1.5 mg N L^{-1} and 0.2 mg L^{-1}, respectively.

Nowadays, with increasing toxic effect of NH_3-N on human health and aquatic organisms, the removal of NH_3-N from wastewater is the main task. NH_3-N They include chemical precipitation (Han, Butterly et al. 2021), photocatalytic oxidation (Yu, Yu et al. 2021), air stripping, break-point chlorination (Zhang, Yin et al. 2022), biological method such as nitrification and denitrification (Adam, Othman et al. 2019), membrane filtration (Rohani, Yusoff et al. 2021), reverse osmosis (Gui, Mai et al. 2020), adsorption (Vocciante, De Folly D'Auris et al. 2018), ion exchange and others (Qin, Zhu et al. 2020). Specifically, ion exchange and adsorption technique are regarded a better choice for treatment NH_3-N contaminated wastewater. This is due to high removal efficiency, ease of application and operation. Moreover, the adsorbents should be effectively low cost, environmentally friendly, practicable alternative properties and

favorable for commercial purpose (Elsherbiny, El-Hefnawy et al. 2017, Huang, Kankanamge et al. 2018).

Large number of adsorbents applied for removal of NH_3-N from wastewater, among of these adsorbents various type of zeolites (Peng, Chai et al. 2017), clays, bentonite (Cheng, Zhu et al. 2019), fly ash (Tang, Xu et al. 2020), activated carbon (Ghany, Ahmed et al. 2017) and synthetic organic resin (Han, Butterly et al. 2021). However, these conventional adsorbents have low adsorption capacity and required secondary physical and chemical treatments that increase the adsorption operation costs (Chen, Zhou et al. 2017). The existence of other competing ions such as (Na^+, K^+, Ca^{2+}) reduce the selectivity of imitative ion exchange resins, the maximum adsorption capacity (q_{max}) of zeolite for removal of NH_4^+ is 1.54 mol kg $^{-1}$, while in the presence of Na^+ removal efficiency decreased from 90% to 36% (Jiang, Minami et al. 2018).

Ligand exchange technology was suggested to enhance the removal efficiency of NH_3-N by ion exchange resins (Chen, Zhou et al. 2017). Cation exchange resin was loaded with metal ion, which formed complex with the polluted substance. The term "ligand exchange" was suggested by Helfferich in 1962, who studied the selectivity of the ion exchanger toward ammonium ion (Chen, Zhou et al. 2017).

The removal of NH_3-N from wastewater by ligand exchange reactions can be represented as the following (Chen, Zhou et al. 2017): -

$$R_2[Cu(H_2O)_4]^{2+} + 4NH_{3(aq)} \rightleftharpoons R_2[Cu(NH_3)_4]^{2+} + 4H_2O \quad (1)$$

Where R denotes the cation exchange resin such as Amberlite IR-120.

Several transition metals such as Cu^{2+}, Ni^{2+}, $Co^{2+,}$ and Zn^{2+} were loaded onto cation exchange resin served as a ligand exchanger (Chen, Zhou et al. 2017, Chen, Chen et al. 2019). There is an electrostatic interaction between active group of ion exchange resin and metal ions. A complex between the metal ion and NH_3-N was formed and NH_3-N replaced the aqua molecule in the solvation shell of metal (Clark and Tarpeh 2020).

There are several studies showed that NH_3-N removal from wastewater using titanate by cation exchange process (Zhang, Wang et al. 2021). Chen Yan et al used Zn(II)-supported on poly ligand exchange resin for the removal of NH_3-N from wastewater (Chen, Chen et al. 2019). It was also removed by high silica zeolite granules regenerated with ozone (Doekhi-Bennani, Leilabady et al. 2021) and manganese oxides (MnOs) (Zhang, Wang et al. 2020). Moreover, Iron oxide nanoparticles dispersed on zeolite by

green synthesis was utilized for the removal of NH_3-N from aqueous solution (Xu, Li et al. 2020).

Strongly cation exchange resins such as Amberlite IR-120 (R-H) used as adsorbent for removal of NH_3-N from wastewater. R-H is sulfonated polystyrene cross-linked with divinylbenzene (Alguacil 2019). It is characteristics by gel form of active site strongly cationic sulfonated group, which plays an essential role in the separation of charged species from aqueous solution. It has thermal stability about 120 °C, high surface area, non-toxic, its total exchange capacity 2 meq/mL, particle size 0.6-0.8 mm (16-45 mesh), and moisture content 45–50 % (Meshram, Sahu et al. 2012, Alguacil 2019).

So, in this work, the removal of NH_3-N from wastewater by ligand exchange technique was studied. R-H was loaded with Cu(II) ions, ($R\text{-}Cu^{2+}$), and used for the removal of NH_3-N from wastewater via the complexation. Afterward, the loaded R-H with copper ammonia complex was applied as a catalyst for the oxidative decolorization of some organic polluted dyes. Therefore, ligand exchange resin has a dual role for consecutive removal of NH_3-N and dyes from wastewater.

2. Experimental

2.1. Materials

Strongly acidic exchange resin, Amberlite IR-120 (R-H) was purchased from Fluka chemie AG, CH-9470 Buchs which was packed in Switzerland. Thymol (5-Methyl-2-isopropylphenol) and sodium nitroprusside dihydrate (pentacyano nitrosyl ferrate II) were purchased from LANXESS AG 50569 cologne (Germany) and used without further purification. Ammonium hydroxide (36 %), sodium hypochlorite (4-5%), acetic acid (99%) were obtained from ADWIC (Egypt). Phosphoric acid (99%) and hydrochloric acid (30%) were purchased from SDFCL (India). Sodium hydroxide, sodium carbonate, sodium hydrogen carbonate, boric acid, cobalt (II) chloride, nickel (II) chloride and copper sulphate were obtained from Sigma-Aldrich. Hydrogen peroxide (50%, as an oxidant) was obtained from Merck (Germany), and potassium permanganate was used to determine its initial concentration (Leonard 1990). Aniline blue (AB), methyl green (MG) and Methyl violet 2B (MV 2B) were purchased from Sigma-Aldrich.

2.2. Instrumental Measurements

The UV/Vis measurements were carried out on a high-performance double beam SPECORD 210 PLUS spectrophotometer with an electronic temperature controller

(Analytic jena, Germany). AD1030 pH-temperature bench meter was used to adjust pH (Adwa, Hungary). Water shaker thermostat (Julabo D-7633 Seelbach, Germany) was used to shake the mixtures during the adsorption process. The concentration of metals was determined by inductively coupled plasma optical emission spectroscopy (ICP-OES) Optima 7000 DV with double monochromator and a simultaneous CCD array detector (Perkin Elmer, USA). The thermogravimetric analysis (TGA) was recorded on Shimadzu TG-50 thermal analyzer (Japan) from 30 °C up to 800 °C with scanning rate of 10 °C min^{-1} under N_2. FT-IR analysis was performed using JASCO FT-IR-4100 (Japan) within the wavenumber range of 4000-400 cm^{-1}. To confirm the structure of the adsorbent, powder X-ray diffraction (XRD) with GNR, APD 2000 PRO diffractometer (Italy) was used. X-ray radiation with Cu-Kα (λ = 1.5405 Å) and operated at 40 kV and 30 mA was directed to the samples. The diffraction patterns were measured within the scanning range of $(4–50^0)2\theta$ with a step size 0.03°. Scanning electron microscope (SEM) measurements were performed with (QUANTA FEG250 microscope). The energy dispersive X-ray spectroscopy (EDX) analysis was investigated using IT100LA operating at an accelerating voltage of 20.00 keV attached to an SEM device.

2.3. Preparation of metal ions supported on ligand exchange resin (R-M^{n+})

An appropriate amount of R-H was washed repeatedly with distilled water to remove any fine particles and non-adhesive impurities, then filtrated and air-dried before used. It was regenerated with (0.1 M HCl) to increase the capacity of the exchanger and then was washed with distilled water to remove excess of Cl^- ions which was detected by $AgNO_3$ test and dried at room temperature for overnight (Salem 2001).

25 g of R-H was dispersed and saturated with 500 ml of $CuSO_4$ solution (0.5 M). This mixture was magnetically stirred for 24 h to achieve the equilibrium state and the resin was converted to Cu^{2+}-form. Afterwards, it was filtered and washed thoroughly with distilled water until the filtrated solution became colorless. The R-Cu^{2+} product was dried in an oven at 50 ºC for 12 h. The loaded amount of Cu (II) ions onto the resin was determined by measuring the concentration of copper ions before and after loading process using ICP spectroscopy (Chen, Chen et al. 2019). R-Ni^{2+} and R-Co^{2+} were similarly prepared using the same circumstances procedure for R-Cu^{2+}.

2.4. Batch equilibrium measurements

To investigate the adsorption capacity of cationic ligand exchange resin (R-M^{2+}) for the removal of NH_3-N from aqueous solution. A fixed amount of R-M^{2+} (0.1 g) was added into a series of Erlenmeyer conical-flasks (100 mL) with stoppers that contain a certain

volume of distilled water (19 mL). A definite volume (1 mL) of ammonia solution (3395 mg/L) was taken by micropipette then added to each flask and all of these flasks were immediately shaken at 130 rpm in shaker water thermostat at controlled temperature 30 ± 0.2 °C for given period. The adsorption capacities of ($R\text{-}M^{2+}$) at different time intervals was defined by determining the concentration of NH_3-N that is free in the solution. The concentration of NH_3-N was determined using indothymol blue method by UV/Vis spectrometer (SPECORD 200 PLUS) (Zamora-Garcia, Correa-Tome et al. 2021).

The removal efficiency percentage, R(%) and the adsorption capacity at time t, q_t (mg/g) of NH_3-N solution onto $R\text{-}M^{2+}$ at different time were estimated using Equs. 2 and 3.

$$R(\%) = \frac{C_o - C_t}{C_o} \text{ x } 100 \quad (2)$$

$$q_t = \frac{(C_o - C_t) \text{ x } V}{m} \quad (3)$$

Where C_o represents the initial concentration of NH_3-N (mg/L), C_t represents the non-adsorbed concentration of NH_3-N, V is the volume of solution (L), and m (g) is the mass of adsorbent.

For $R\text{-}Cu^{2+}$ as an adsorbent, the influence of temperature on NH_3-N uptake was performed at 20, 30 and 40 ^oC ± 0.2 ^oC, respectively using fixed initial NH_3-N concentration and amount of $R\text{-}Cu^{2+}$ (0.1 g). Universal buffers of pH range from 2 to 12 were utilized to know the impact of pH in the removal efficiency of NH_3-N.

2.5. Catalytic oxidation of dyes

The recovery and reusability of R/Cu(II)-amine composite after washing with distilled water several times and drying in oven at 50 ^oC for 12 h were studied. It was used for catalytic decolorization of different types of dyes by the oxidation process. The stock solutions (1×10^{-3} mol L^{-1}) of AB, (5×10^{-4} mol L^{-1}) of MG, and (2.4×10^{-3} mol L^{-1}) of MV2B dyes were prepared. The optimum reaction mixture was set up in a 100 mL Erlenmeyer flask, which containing known concentration of mixture of the dye and appropriate concentration of H_2O_2 solution. The flasks were put in a water shaker thermostat at 30 ^oC ± 1 ^oC and agitated at 120 rpm for a given period. A specific amount of R-Cu (II) amine composite (0.05 g) was added, and the change of the absorbance of each dye solution was determined with time.

The decolorization efficiency was determined using Equ. 4

$$\text{Removal efficiency (\%)} = \frac{A_o - A_t}{A_o} \times 100 \quad (4)$$

Where, A_o is the initial absorbance of dye (at time 0) and A_t is the absorbance at time t (min).

3. Results and discussion

3.1. Loading of metal ions on R-H

R-H was loaded with different amounts of copper (II), nickel (II) and Co (II) as measured by ICP spectroscopy. It was found that 1g of R-H has been loaded with 245.6 mg L^{-1}, 52.8 mg L^{-1}, and 10 mg L^{-1} of copper (II), nickel (II) and Co (II), respectively. This can be attributed to the selectivity of the sulfonate (-SO_3H) functional group of R-H towards loaded metal ions. It was written that this selectivity increases with increasing the atomic size of metal ions (Chandrasekara and Pashley 2015). The ionic radius of three metals decreases according to the order Cu(II) > Ni(II) > Co(II). As a result, the highest loaded amount on R-H was found for Cu(II).

3.2. Characterization

3.2.1. FT-IR

The FTIR spectra of R-H, R-Cu^{2+} and R-Cu^{2+} after adsorption of NH_3-N (R/Cu(II)-amine composite) are shown in Fig. 1(a). For parent R-H, there is a stretching vibration of O–H groups which originated from H_2O molecule due to moisture are shown around 3434 cm^{-1}. The peaks at 2920 cm^{-1} are corresponded to the symmetric and asymmetric C–H stretching vibration of C–H and –CH_2 groups, the peaks observed at 2370 cm^{-1} is due to O–H stretching mode that is originated from the polymer (Singare, Lokhande et al. 2011). The band at 1637 cm^{-1} indicates C=C stretching vibration of aromatic rings, stretching vibration of O–S–O group of sulfonic acid was recorded at 1388 cm^{-1} and the peaks observed at 1170 cm^{-1} and 999 cm^{-1} are represented to symmetric stretching of –SO_3 group (Prekob, Hajdu et al. 2019). The band at 835 cm^{-1} represented bending C–H out-of-plane deformation of the aromatic ring and at 679 cm^{-1} attributed to –SO_3H groups (Ghosh, Dhole et al. 2015). The stretching –OH peak at 3434 cm^{-1} was shifted to 3460 cm^{-1} and 3468 cm^{-1} according to (R-Cu^{2+}) and R/Cu(II)-amine composite, respectively. The intensity of C=C was strengthened in case of (R-Cu^{2+}) and (R/Cu(II)-amine composite). The change in the intensity of peaks at 1172 cm^{-1}, 1036 cm^{-1} and 833 cm^{-1} due to the complex formation between Cu (II) ion and –SO_3H groups (Jha, Van Nguyen et al. 2009). After the complexation of ammonia with Cu^{2+}, the peak of SO_2 group further shifted from 1388 cm^{-1} to1401 cm^{-1} and a new band appeared at 517 cm^{-}

[1] due to the stretching vibration of N–Cu which confirm the complex formation between Cu (II) ion and ammonia in solution (Chen, Chen et al. 2019).

3.2.2. XRD analysis

Figure 1(b) presents that the X-ray diffractogram of R-H which has a narrow diffuse peak in the spectrum, indicating that it is amorphous in nature (Yousef and Malika 2020). In case of R-Cu^{2+}, the main peak of Amberlite IR-120 ($2\theta = 18.6°$) was shifted to lower value ($2\theta = 15.6°$) due to the loading of Cu^{2+} on the surface of Amberlite IR-120 (Manivannan, Starvin et al. 2010). A new peak was appeared at ($2\theta = 23.3°$) due to the complexation between Cu^{2+} and ammonia in solution with keeping the amorphous nature of R-H.

3.2.3. TGA

Thermal stability of R/Cu(II)-amine composite was investigated via TGA technique as displayed in Fig. 1(c). The thermogram of R/Cu(II)-amine composite demonstrated that the total loss of weight of about 93.08 % in three separate steps. The first step showed about 19.42 % loss of weight at the temperature range of 28-100 ^{o}C. This is attributed to the evaporation of adsorbed water molecules from the surface. The second step represents the complete decomposition of amino ligand in the complex of Cu (II)–amine with a weight loss of 9.677 % in the range of 100–295 ^{o}C (Jeslin Kanaga Inba, Annaraj et al. 2013). The last weight loss step was noted above 295 ^{o}C with 63.96 % degradation. This corresponds to the degradation of organic polymer of R-H leaving thermally stable metal oxide as a residue (Singare, Lokhande et al. 2011).

3.2.4. SEM

The surface morphology of R-H, R-Cu^{2+}, and R/Cu(II)-amine complex was investigated by SEM, Fig. 2(a, b, c). The surface of pure R-H is a plane spherical structure. But in the case of R-Cu^{2+}, it was observed that some grains have generated on its surface which indicates the impregnation of R-H with Cu^{2+} (Singare, Lokhande et al. 2011). Also, the grain species turned to be a coarse coating at the surface of R/Cu(II)-amine composite which indicated the complex formation between ammonia and the Cu^{2+} ions at the surface of R-Cu^{2+}.

3.2.5. EDX

The adsorption of ammonium ions on the surface of R-Cu^{2+} was confirmed by EDX measurement. Figure 2(d) presents the EDX spectra of R/Cu(II)-amine composite. EDX

composition analysis for R/Cu(II)-amine complex indicate the presence of C, N, O, S, and Cu elements, Table (1).

3.3. Kinetics of NH_3-N removal by metal ions supported on ligand exchange resin (R-M^{n+})

A comparison study between the removal efficiency of NH_4^+ using R-Cu^{2+}, R-Ni^{2+}, and R-Co^{2+}, at the same initial concentration of NH_4^+ was carried out. It was found that the uptake amount of NH_4^+ by R-Cu^{2+} (q_e = 200 mg/g) more than that by R-Ni^{2+} (q_e = 158.55 mg/g) and by R-Co^{2+} (q_e = 143.18 mg/g), as shown in Fig. 3(b). The highest removal efficiency in the case of R-Cu^{2+} can be attributed to the highest loaded concentration of Cu^{2+} ion on the surface of R-H than Ni^2 and Co^{2+} (Demirbas, Pehlivan et al. 2005). So, R-Cu^{2+} was established as the best adsorbent which can be applied for the removal of NH_3-N from wastewater. So, detailed experiments concentrated on the removal efficiency of NH_4^+ using R-Cu^{2+} were achieved under different conditions.

The adsorbed amount of NH_4^+ onto R-Cu^{2+} changing within time. It was increased sharply in the first 20 min and attained the equilibrium state within 50 min, Fig. 3(a). The initial rapid adsorption of NH_3-N onto R-Cu^2 can be assigned to large number of the exchangeable active sites which increase the complexation's rate between loaded Cu^{2+} ions and NH_3-N in solution. After that, the adsorption process became slower and slower till reached the equilibrium due to no vacant Cu^{2+} ions on the surface. The maximum adsorption capacities (q_{max}) of NH_4^+ on various other adsorbents reported in the literature are shown in Table (2). R-Cu^{2+} has the highest the adsorption capacity of NH_4^+, reflecting that R-Cu^{2+} is a good candidate for the removal of NH_4^+ from aqueous solution.

Three kinetic models namely, pseudo-first-order, pseudo-second-order and intraparticle diffusion models (Eqs. 5, 6 and 7, respectively) are applied to find out the relation between NH_3-N concentration and adsorption rate and fitting the experimental data of adsorption (Cheng, Zhu et al. 2019).

$$\ln(q_e - q_t) = \ln q_e - k_1 t \quad (5)$$

$$\frac{t}{q_t} = \frac{1}{k_2 q_e^2} + \frac{t}{q_e} \quad (6)$$

$$q_t = k_p t^{1/2} + C \quad (7)$$

Where, q_e and q_t (mg/g) are the adsorbed amount of NH_3-N at equilibrium and at contact time t, respectively. k_1 (min^{-1}), k_2 (g/mg min) and k_p ($mg.g^{-1}.min^{1/2}$) are the rate constant of pseudo-first-order, pseudo-second-order and the intra-particle diffusion,

respectively. C ($mg.g^{-1}$) is a constant term that represents the thickness of the boundary layer.

The values of kinetic parameters, the correlation coefficient, R^2, and the calculated adsorption capacity ($q_{e,cal}$) were presented in Table (3). According to this Table, the adsorption of NH_3-N onto R-Cu^{2+} does not fit the pseudo-first-order model due to the low value of the correlation coefficient ($R^2 \approx 0.81$). In addition, the values of ($q_{e,cal}$) and the experimental one ($q_{e,exp}$) were not compatible. However, the calculate ($q_{e,cal}$) from the pseudo-second-order equation was matched with the experimental one ($q_{e,exp}$). Additionally, the value of (R^2) was close to unity, indicating that pseudo-second-order model is the best one to describe the adsorption of NH_3-N from an aqueous solution onto the surface of R-Cu^{2+}. Moreover, the adsorption mechanism was carried out by the chemical adsorption process (Zhang, Wang et al. 2020). The fitting data of the intraparticle diffusion model involved two steps as presented in Fig. 4, indicating that the adsorption mechanism was involve two steps. The first step was mainly due to the film diffusion and the fitting lines away from origin implying that the adsorption of NH_3-N occurring over the external surface. Therefore, the intraparticle diffusion was not the rate-controlling step. The second step was assigned to the intraparticle diffusion (Elsherbiny, Gemeay et al. 2020). The values of k_{p1} and k_{p2} are listed in Table (3), where the value of k_{p1} is greater than that of k_{p2}.

3.4. Impact of pH

pH of the medium is one of the most critical factors for the removal of NH_3-N by R-Cu^{2+}. Since it possesses a significant role of the ratio of two forms of ammonia and the adsorbent surface. The impact of pH in the removal of NH_3-N was examined in the pH range from 2 to 12 using universal buffer, while the initial concentration of NH_3-N, amount of R-Cu^{2+} and temperature were kept constant, Fig. 5. NH_3-N in an aqueous solution is available in two forms, ammonium ion (NH_4^+) and unionized ammonia (NH_3) and the proportion of both forms depends on pH and temperature. At the pH lower than 4, the amount of NH_3-N uptake is slightly increased, this is due to the predominant form of ammonia in this range is NH_4^+. On the other hand, when the pH increases from 4 to 8, the removal efficiency increased significantly from 10.6 % to 65.2 %. This increasing is attributed to ammonium ion is gradually converted to NH_3 which react with Cu^{2+} to form Cu (II)-amine complex as shown in eq (1). However, above pH 8, the NH_3-N removal efficiency decreased, because of the considerably increasing in the concentration of hydroxide ion developed in alkaline medium. This

increasing can be form a precipitate of copper (II) hydroxide $Cu(OH)_2$, which leads to decrease the amount of copper loaded on the resin (Chen, Chen et al. 2019).

3.5. Effect of R-Cu^{2+} dose

The effect of the amount of R-Cu^{2+} on the removal efficiency of NH_3-N was carried out using the variable amounts of R-Cu^{2+} and the other factors were kept constant. As the amount of R-Cu^{2+} increased, the amount of NH_3-N uptake increased significantly as shown in Fig. 6. It was noticed that the removal efficiency increased from 32.7 to 90.8 % as the amount of R-Cu^{2+} increased from 0.02 g to 0.2 g, respectively. This increment is due to the large surface area of the adsorbent and increasing the adsorbent dose which in turn leads to increase the number of exchangeable active site. Moreover, the loading copper concentration increased so that the rate of complexation between metal and NH_3-N increased (Clark and Tarpeh 2020).

3.6. Impact of initial NH_3-N concentration.

The impact of the initial NH_3-N concentration $[NH_4^+]_o$ was studied by changing its concentration between 398.6 to 1686.18 mg. L^{-1}, Fig. 7. The removal efficiency of NH_3-N using R-Cu^{2+} at given time increases from 89.22 to 93.98 % as the initial concentration of NH_3-N increases from 398.6 to 1686.18 mg. L^{-1}. This is due to an enhancement of the concentration gradient of NH_3-N in solution that leads to a large mass transfer driving force (Wang, Xu et al. 2020). Also, the available adsorption active site of adsorbent (R-Cu^{2+}), becomes fewer due to continuous blocking of this site with NH_3-N to form (R/Cu(II)-amine composite). on the other hand, some of ammonia molecules don't get absorbed and remain free in the solution (Ding and Sartaj 2016).

3.7. Adsorption isotherms models

To obtain information about the distribution of adsorbate molecules between the liquid phase and solid phase at the equilibrium state, adsorption isotherm was studied. NH_3-N adsorption isotherm has been investigated at several initial concentrations and three different temperatures. The adsorption isotherm was evaluated using four models, Freundlich, Langmuir, Temkin and Dubinin-Radushkevich (D-R) isotherms (Eqs. 8, 9, 10, and 11, respectively).

$$\frac{C_e}{q_e} = \frac{C_e}{q_{max}} + \frac{1}{q_{max}\, K_L} \tag{8}$$

$$\ln q_e = \frac{1}{n} \ln C_e + \ln K_F \tag{9}$$

$$q_e = B_1 \mathrm{Ln} K_T + B_1 \mathrm{Ln} C_e \tag{10}$$

$$\mathrm{Ln}q_e = \mathrm{Ln}q_m - B\varepsilon^2 \quad (11)$$

Where, C_e (mg L^{-1}) is the concentration of NH_3-N at equilibrium, q_{max} (mg/g) is the maximum adsorption capacity of NH_3-N and K_L (L/mg) is Langmuir adsorption constant that is related to the adsorption energy (Doekhi-Bennani, Leilabady et al. 2021). K_F (mg/g) and 1/n are Freundlich constants related to the adsorption capacity and adsorption intensity, respectively. K_T (L/mg) is the Temkin equilibrium constant that is connected to the maximum binding energy, and B_1 (J/mol) is a constant representing the heat of adsorption which is calculated from the following expression B = RT/b; R is the gas constant, T is the absolute temperature (K), and b is the adsorption potential (Chen, Zhou et al. 2017). q_m is the monolayer capacity (mg g^{-1}), and ε is the Polanyi's potential. The value of ε can be written as: $\varepsilon = RT \ln[1 + 1/C_e]$. The value of B gained from the slope of D-R's plot is utilized to calculate the mean adsorption energy (E, kJ/mol) which was obtained from the following equation:

$$E = 1/(-2B)^{0.5} \quad (12)$$

All parameters obtained from the isotherm models along with their correlation coefficient (R^2) were listed in Table (4). By comparing the values of (R^2) it was found that the adsorption NH_3-N on R-Cu^{2+} not obeyed Langmuir model. Whereas, it can be described by Freundlich, Temkin and D-R models. The highest value of (R^2) was found that of the Freundlich model, revealing that the Freundlich model is the best one for representing the adsorption process with a formation of the monolayer coverage. According to the data in Table (4), the values of (1/n) were larger than unity and decreased with increasing the temperature, indicating the adsorption process becomes less unfavorable at higher temperatures. However, the K_F values increase with increasing temperature. This suggesting that the adsorption process is of an endothermic nature and favorable at higher temperatures (Fu, Zhao et al. 2021).

From Temkin model, it was found that, the value of B_1 decreased with increasing the temperature (Elsherbiny, Gemeay et al. 2020). In addition, the better fitting results of Temkin model indicated that the adsorption of NH_3-N is dominated by chemisorption, which is in agreement with the results of pseudo-second-order model. The value of E, which was calculated form D-R model gives information about the mechanism of adsorption. Its value was higher than 20 kJ/mol, indicating the adsorption of NH_3-N onto R-Cu^{2+} is governed by chemical adsorption (Elsherbiny, Gemeay et al. 2020) coinciding with Temkin model. This value confirms that the removal of ammonia from

aqueous solution using R-Cu^{2+} was through complexation and R/Cu(II)-amine composite was formed. Additionally, this value was increased with increasing the temperature.

3.8. Thermodynamic parameters

Deep insight on the changes in the energetic parameters related to the adsorption process was provided from thermodynamic studies. The parameters of adsorption thermodynamics can be calculated by introducing the experimental data at three different temperatures into the following Equations (Elsherbiny 2013).

$$\ln K_d = -\frac{\Delta H_{ads}}{RT} + \frac{\Delta S_{ads}}{R} \quad (13)$$

$$\Delta G_{ads} = -RT \ln K_d \quad (14)$$

$$\Delta G_{ads} = \Delta H_{ads} - T\Delta S_{ads} \quad (15)$$

Where; K_d is the distribution coefficient ($K_d = q_e/C_e$), ΔG_{ads} is the change in Gibbs-free energy of adsorption process, ΔH_{ads} (kJ.mol^{-1}) is the enthalpy change, and ΔS_{ads} (J.mol^{-1}.K^{-1}) is the entropy change. The distribution coefficient (K_d) and the thermodynamic parameters were presented in Table 5. As shown in Table 5, the value of K_d enhanced as temperature increased from 293 to 313 K. The values of ΔS_{ads} and ΔH_{ads} were determined by plotting Van't Hoff 's equation (Eq. 13). The positive value of ΔH_{ads} indicates endothermic nature of the adsorption process. While, the positive value of ΔS_{ads} revealed that the degree of disorder increased at solid-liquid interface during the adsorption of NH_3-N onto R-Cu^{2+} (Pan, Zhang et al. 2019). The negative values of ΔG_{ads} demonstrated that the adsorption of NH_3-N is a feasible and spontaneous process. Furthermore, the value of ΔG_{ads} becomes more negative with increasing the temperature, suggests the adsorption of NH_3-N onto R-Cu^{2+} was more favorable and spontaneous at higher temperatures.

3.9. Catalytic activity application of R/Cu(II)-amine composite for the oxidative degradation of dyes

Wastewater discharge during dyes manufacturing and textile dyeing cause serious problems for both the environment and human life. This type of pollutant is produced by manufacturing poisonous and potential carcinogenic materials, that contain highly colored organic compounds that have a low degradation ability (Salem, El-Ghamry et al. 2014).

The valorization of the resulting product R/Cu(II)-amine composite was carried out. This product was applied to remove three different organic dyes namely, aniline blue

(AB), methyl green (MG), and methyl violet (MV 2B) from aqueous solution. The removal of these dyes was done in the presence of H_2O_2 as an eco-friendly oxidant. Fig. 8, presents the time decay of the absorbance of the three dyes. A glance to Fig. 8, the color of MG dye was completely disappeared in about 40 min. However, about 92.64 % and 90.26 % of AB and MV dyes were removed after 80 min. These results confirmed the ability of R/Cu(II)-amine composite as an efficient catalyst for removal of both anionic and cationic dyes from wastewater.

4. Conclusion

In conclusion, Amberlite IR-120 (R-H) was successfully loaded with Cu^{2+}, Ni^{2+} and Co^{2+} through cation exchange mechanism to form R-M^{n+}. The highest loaded amount was found in case of Cu^{2+} with value of 245.6 mg L^{-1} for 1g of R-H. The loaded resin R-M^{n+} was applied to get rid of ammonia from aqueous solution and the highest removal efficiency was found in the case of R-Cu^{2+}. The adsorption of NH_3-N from an aqueous solution onto the surface of R-Cu^{2+} obeyed pseudo-second-order model and Freundlich isotherm. The removal mechanism was governed by chemical adsorption and formation of R/Cu(II)-amine composite. The formed R/Cu(II)-amine composite was used as an efficient catalyst for removal of aniline blue, methyl green, and methyl violet dyes from aqueous solution in presence of H_2O_2.

Ethical Approval

Not applicable

Consent to Participate

All the authors are agreed to participate in this work

Consent to Publish

All the authors are agreed to publish this work in *Environmental Science and Pollution Research*

Authors Contributions

Marwa A. El-Ghobashy, Mohamed M. Khamis, Abeer S. Elsherbiny, Ibrahim A. Salem: validation; Marwa A. El-Ghobashy, Mohamed M. Khamis, Abeer S. Elsherbiny: formal analysis; Mohamed M. Khamis: investigation and data curation; Abeer S. Elsherbiny, Marwa A. El-Ghobashy, Mohamed M. Khamis: writing-original draft preparation; Marwa A. El-Ghobashy, Abeer S. Elsherbiny: review and editing; Ibrahim A. Salem; Put the idea of the work and final revision.

Funding

This research has received no fund from any source.

Competing Interests

There are no conflicts to declare

Availability of data and materials

All the data and materials are available in the manuscript

References

Adam, M. R., M. H. D. Othman, R. Abu Samah, M. H. Puteh, A. F. Ismail, A. Mustafa, M. A. Rahman and J. Jaafar (2019). "Current trends and future prospects of ammonia removal in wastewater: A comprehensive review on adsorptive membrane development." Separation and Purification Technology **213**: 114-132.

Alguacil, F. J. (2019). "The removal of toxic metals from liquid effluents by ion exchange resins. Part IX: Lead(II)/H+/Amberlite IR-120." Revista de Metalurgia **55**(1).

Chandrasekara, N. P. G. N. and R. M. Pashley (2015). "Study of a new process for the efficient regeneration of ion exchange resins." Desalination **357**: 131-139.

Chen, Q., K. Zhou, Y. Chen, A. Wang and F. Liu (2017). "A novel poly ligand exchanger - Cu(II)-loaded chelating resin for the removal of ammonia-nitrogen in aqueous solutions." Environ Technol **38**(22): 2824-2834.

Chen, Q., K. Zhou, Y. Chen, A. Wang and F. Liu (2017). "Removal of ammonia from aqueous solutions by ligand exchange onto a Cu(ii)-loaded chelating resin: kinetics, equilibrium and thermodynamics." RSC Advances **7**(21): 12812-12823.

Chen, Q., K. Zhou, Y. Hu, F. Liu and A. Wang (2017). "Effect of competing ions and causticization on the ammonia adsorption by a novel poly ligand exchanger (PLE) ammonia adsorption reagent." Water Sci Technol **75**(5-6): 1294-1308.

Chen, Y., W. Chen, Q. Chen, C. Peng, D. He and K. Zhou (2019). "Removal of ammonia-nitrogen in wastewater using a novel poly ligand exchanger-Zn(II)-loaded chelating resin." Water Sci Technol **79**(1): 126-136.

Cheng, H., Q. Zhu and Z. Xing (2019). "Adsorption of ammonia nitrogen in low temperature domestic wastewater by modification bentonite." Journal of Cleaner Production **233**: 720-730.

Clark, B. and W. A. Tarpeh (2020). "Selective Recovery of Ammonia Nitrogen from Wastewaters with Transition Metal-Loaded Polymeric Cation Exchange Adsorbents." Chemistry **26**(44): 10099-10112.

Demirbas, A., E. Pehlivan, F. Gode, T. Altun and G. Arslan (2005). "Adsorption of Cu(II), Zn(II), Ni(II), Pb(II), and Cd(II) from aqueous solution on Amberlite IR-120 synthetic resin." J Colloid Interface Sci **282**(1): 20-25.

Ding, Y. and M. Sartaj (2016). "Optimization of ammonia removal by ion-exchange resin using response surface methodology." International Journal of Environmental Science and Technology **13**(4): 985-994.

Doekhi-Bennani, Y., N. M. Leilabady, M. Fu, L. C. Rietveld, J. P. van der Hoek and S. G. J. Heijman (2021). "Simultaneous removal of ammonium ions and sulfamethoxazole by ozone regenerated high silica zeolites." Water Res **188**: 116472.

Elkady, M., E. Salama, W. A. Amer, E. M. Ebeid, M. M. Ayad and H. Shokry (2020). "Novel eco-friendly electrospun nanomagnetic zinc oxide hybridized PVA/alginate/chitosan nanofibers for enhanced phenol decontamination." Environ Sci Pollut Res Int **27**(34): 43077-43092.

Elsherbiny, A. S. (2013). "Adsorption kinetics and mechanism of acid dye onto montmorillonite from aqueous solutions: Stopped-flow measurements." Applied Clay Science **83-84**: 56-62.

Elsherbiny, A. S., M. E. El-Hefnawy and A. H. Gemeay (2017). "Adsorption Efficiency of Polyaspartate-Montmorillonite Composite Towards the Removal of Pb(II) and Cd(II) from Aqueous Solution." Journal of Polymers and the Environment **26**(2): 411-422.

Elsherbiny, A. S., A. H. Gemeay and M. A. Salem (2020). "Adsorption efficiency of graphene oxide towards cyanine dyes with different alkyl chain lengths." Separation Science and Technology **56**(2): 266-274.

Fu, G., Y. Zhao, S. Zhou, C. Chen, Y. Zhong and Y. Xu (2021). "Efficient removal of nitrogen and phosphorus in aqueous solutions using modified water treatment residuals-sodium alginate beads." Environ Sci Pollut Res Int.

Ghany, H. A., M. Ahmed and E. Ashour (2017). "Adsorption of Ammonia onto Activatedcarbon Prepared from Rice Straw." International Journal of Advanced Research **5**(2): 1180-1196.

Ghosh, S., K. Dhole, M. K. Tripathy, R. Kumar and R. S. Sharma (2015). "FTIR spectroscopy in the characterization of the mixture of nuclear grade cation and anion exchange resins." Journal of Radioanalytical and Nuclear Chemistry **304**(2): 917-923.

Gui, S., Z. Mai, J. Fu, Y. Wei and J. Wan (2020). "Transport Models of Ammonium Nitrogen in Wastewater from Rare Earth Smelteries by Reverse Osmosis Membranes." Sustainability **12**(15).

Han, B., C. Butterly, W. Zhang, J.-z. He and D. Chen (2021). "Adsorbent materials for ammonium and ammonia removal: A review." Journal of Cleaner Production **283**.

Huang, J., N. R. Kankanamge, C. Chow, D. T. Welsh, T. Li and P. R. Teasdale (2018). "Removing ammonium from water and wastewater using cost-effective adsorbents: A review." J Environ Sci (China) **63**: 174-197.

Jeslin Kanaga Inba, P., B. Annaraj, S. Thalamuthu and M. A. Neelakantan (2013). "Cu(II), Ni(II), and Zn(II) Complexes of Salan-Type Ligand Containing Ester Groups: Synthesis, Characterization, Electrochemical Properties, and In Vitro Biological Activities." Bioinorg Chem Appl **2013**: 439848.

Jha, M. K., N. Van Nguyen, J.-c. Lee, J. Jeong and J.-M. Yoo (2009). "Adsorption of copper from the sulphate solution of low copper contents using the cationic resin Amberlite IR 120." Journal of Hazardous Materials **164**(2-3): 948-953.

565 Jiang, Y., K. Minami, K. Sakurai, A. Takahashi, D. Parajuli, Z. Lei, Z. Zhang and T.
566 Kawamoto (2018). "High-capacity and selective ammonium removal from water using
567 sodium cobalt hexacyanoferrate." RSC Advances **8**(60): 34573-34581.
568
569 Karri, R. R., J. N. Sahu and V. Chimmiri (2018). "Critical review of abatement of
570 ammonia from wastewater." Journal of Molecular Liquids **261**: 21-31.
571
572 Leonard, M. A. (1990). "Vogel's textbook of quantitative chemical analysis. 5th edn:
573 Revised by G. H. Jeffery, J. Bassett, J. Mendham and R. C. Denney. Pp. 877. Longman,
574 Harlow. 1989. £34.00." Endeavour **14**(2): 100.
575
576 Liu, H., Z. Chen, Y. Guan and S. Xu (2018). "Role and application of iron in water
577 treatment for nitrogen removal: A review." Chemosphere **204**: 51-62.
578 Manivannan, D., M. Starvin and V. M. Biju (2010). "Preconcentration of Cu (II) from
579 seawater using a novel and stable phenol-formaldehyde resin." Water Sci Technol
580 **61**(7): 1853-1863.
581
582 Meshram, P., S. K. Sahu, B. D. Pandey, V. Kumar and T. R. Mankhand (2012).
583 "Removal of Chromium(III) from the Waste Solution of an Indian Tannery by
584 Amberlite IR 120 Resin." International Journal of Nonferrous Metallurgy **01**(03): 32-
585 41.
586
587 Pan, M., M. Zhang, X. Zou, X. Zhao, T. Deng, T. Chen and X. Huang (2019). "The
588 investigation into the adsorption removal of ammonium by natural and modified
589 zeolites: kinetics, isotherms, and thermodynamics." Water SA **45**(4 October).
590
591 Peng, C., L.-Y. Chai, C.-J. Tang, X.-B. Min, M. Ali, Y.-X. Song and W.-M. Qi (2017).
592 "Feasibility and enhancement of copper and ammonia removal from wastewater using
593 struvite formation: a comparative research." Journal of Chemical Technology &
594 Biotechnology **92**(2): 325-333.
595
596 Prekob, Á., V. Hajdu, G. Muránszky, I. Kocserha, B. Fiser, B. Viskolcz and L.
597 Vanyorek (2019). "Application of carbonized ion exchange resin beads as catalyst
598 support for gas phase hydrogenation processes." Reaction Kinetics, Mechanisms and
599 Catalysis **129**(1): 85-94.
600
601 Qin, Y., X. Zhu, Q. Su, A. Anumah, B. Gao, W. Lyu, X. Zhou, Y. Xing and B. Wang
602 (2020). "Enhanced removal of ammonium from water by ball-milled biochar." Environ
603 Geochem Health **42**(6): 1579-1587.
604
605 Rohani, R., I. I. Yusoff, N. Khairul Zaman, A. Mahmood Ali, N. A. B. Rusli, R. Tajau
606 and S. A. Basiron (2021). "Ammonia removal from raw water by using adsorptive
607 membrane filtration process." Separation and Purification Technology **270**.
608
609 Salem, I. A. (2001). "Activation of H2O2 by Amberlyst-15 resin supported with
610 copper(II)-complexes towards oxidation of crystal violet." Chemosphere **44**(5): 1109-
611 1119.
612

Salem, I. A., H. A. El-Ghamry and M. A. El-Ghobashy (2014). "Catalytic decolorization of Acid blue 29 dye by H2O2 and a heterogeneous catalyst." Beni-Suef University Journal of Basic and Applied Sciences **3**(3): 186-192.

Singare, P. U., R. S. Lokhande and R. S. Madyal (2011). "Thermal Degradation Studies of Some Strongly Acidic Cation Exchange Resins." Open Journal of Physical Chemistry **01**(02): 45-54.

Tang, H., X. Xu, B. Wang, C. Lv and D. Shi (2020). "Removal of Ammonium from Swine Wastewater Using Synthesized Zeolite from Fly Ash." Sustainability **12**(8).

Vocciante, M., A. De Folly D'Auris, A. Finocchi, M. Tagliabue, M. Bellettato, A. Ferrucci, A. P. Reverberi and S. Ferro (2018). "Adsorption of ammonium on clinoptilolite in presence of competing cations: Investigation on groundwater remediation." Journal of Cleaner Production **198**: 480-487.

Wang, G., Y. Xu, C. Wang, Y. Gao and L. Li (2020). "Synthesis of Two Kinds of Mesoporous Diatomite by Microwave Assisted Sol-Gel Method and Its Adsorption of Ammonia Nitrogen in Wastewater." IOP Conference Series: Materials Science and Engineering **782**.

Xu, Q., W. Li, L. Ma, D. Cao, G. Owens and Z. Chen (2020). "Simultaneous removal of ammonia and phosphate using green synthesized iron oxide nanoparticles dispersed onto zeolite." Sci Total Environ **703**: 135002.

Yousef, R. and C. Malika (2020). "Sorption behavior and mechanism of oxytetracycline from simulated wastewater by Amberlite IR-120 resin." Water Sci Technol **82**(11): 2366-2380.

Yu, R., X. Yu, J. Fu, Y. Zhang, Y. Liu, Y. Zhang and S. Wu (2021). "Removal of ammonia nitrogen in aquaculture wastewater by composite photocatalyst TiO2/carbon fibre." Water and Environment Journal.

Zamora-Garcia, I., F. E. Correa-Tome, U. H. Hernandez-Belmonte, V. Ayala-Ramirez and J.-P. Ramirez-Paredes (2021). "Mobile digital colorimetry for the determination of ammonia in aquaculture applications." Computers and Electronics in Agriculture **181**.

Zhang, L., J. Wang, H. Qiao, F. Liu and Z. Fu (2020). "Synthesis of manganese oxides for adsorptive removal of ammonia nitrogen from aqueous solutions." Journal of Cleaner Production **272**.

Zhang, W., Z. Wang, Y. Liu, J. Feng, J. Han and W. Yan (2021). "Effective removal of ammonium nitrogen using titanate adsorbent: Capacity evaluation focusing on cation exchange." Sci Total Environ **771**: 144800.

Zhang, Y., S. Yin, H. Li, J. Liu, S. Li and L. Zhang (2022). "Treatment of ammonia-nitrogen wastewater by the ultrasonic strengthened break point chlorination method." Journal of Water Process Engineering **45**.

Zhu, Y., J. Chen, D. Yuan, Z. Yang, X. Shi, H. Li, H. Jin and L. Ran (2019). "Development of analytical methods for ammonium determination in seawater over the last two decades." TrAC Trends in Analytical Chemistry **119**.

Legends of Figures

Fig.1. (a) FT-IR spectra of R-H, R-Cu^{2+}, and R/Cu(II)-amine composite**;** (b) XRD patterns of R-H, R-Cu^{2+}, and R/Cu(II)-amine composite; (c) TGA curve of R/Cu(II)-amine composite.

Fig. 2. (a) SEM images of R-H; (b) SEM images of R-Cu^{2+}; (c) SEM images of R/Cu(II)-amine composite; (d) EDX image of R/Cu(II)-amine composite.

Fig. 3. (a) Effect of contact time on the adsorption capacities of NH_4^+; (b) The removal efficiency of NH_4^+ onto R-Cu^{2+}, R-Ni^{2+} and R-Co^{2+} (0.1 g) using $[NH_4^+]_o$ =1060 mg. L^{-1}, 130 rpm and 30 ^oC.

Fig. 4. Intra-particle diffusion plot of the adsorption of NH_4^+ onto (0.1 g) of R-Cu^{+2} at 30 ^oC.

Fig. 5. The effect of initial pH on the removal efficiency of NH_3-N, $[NH4^+]_o$ = 1032.9 mg. L^{-1} using R-Cu^{2+} (0.1 g) at 30 ^oC.

Fig. 6. The effect of dose (R-Cu^{2+}) on the removal efficiency of NH_3-N, $[NH4^+]_o$ = 1032.9 mg. L^{-1}, pH = 8.6 and temperature 30 ^oC.

Fig. 7. Influence of initial concentration of NH_3-N solution on the removal efficiency at different time using R-Cu^{2+}= 0.1 g, pH= 8.6 at 30 ^oC.

Fig. 8. Absorbance-time plots for the catalytic degradation of different types of organic dyes using 0.05 g of R/Cu(II)-amine composite as a catalyst in the presence of $[H_2O_2]$ = 0.01 mol L^{-1} at 30 °C: **(A)** [MV] = 1.86 x 10^{-4} mol L^{-1}, **(B)** [AB]= 7.5 x 10^{-5} mol L^{-1}, and **(C)** [MG]= 2.5 x 10^{-5} mol L^{-1}.

706 **Graphical Abstract**

707

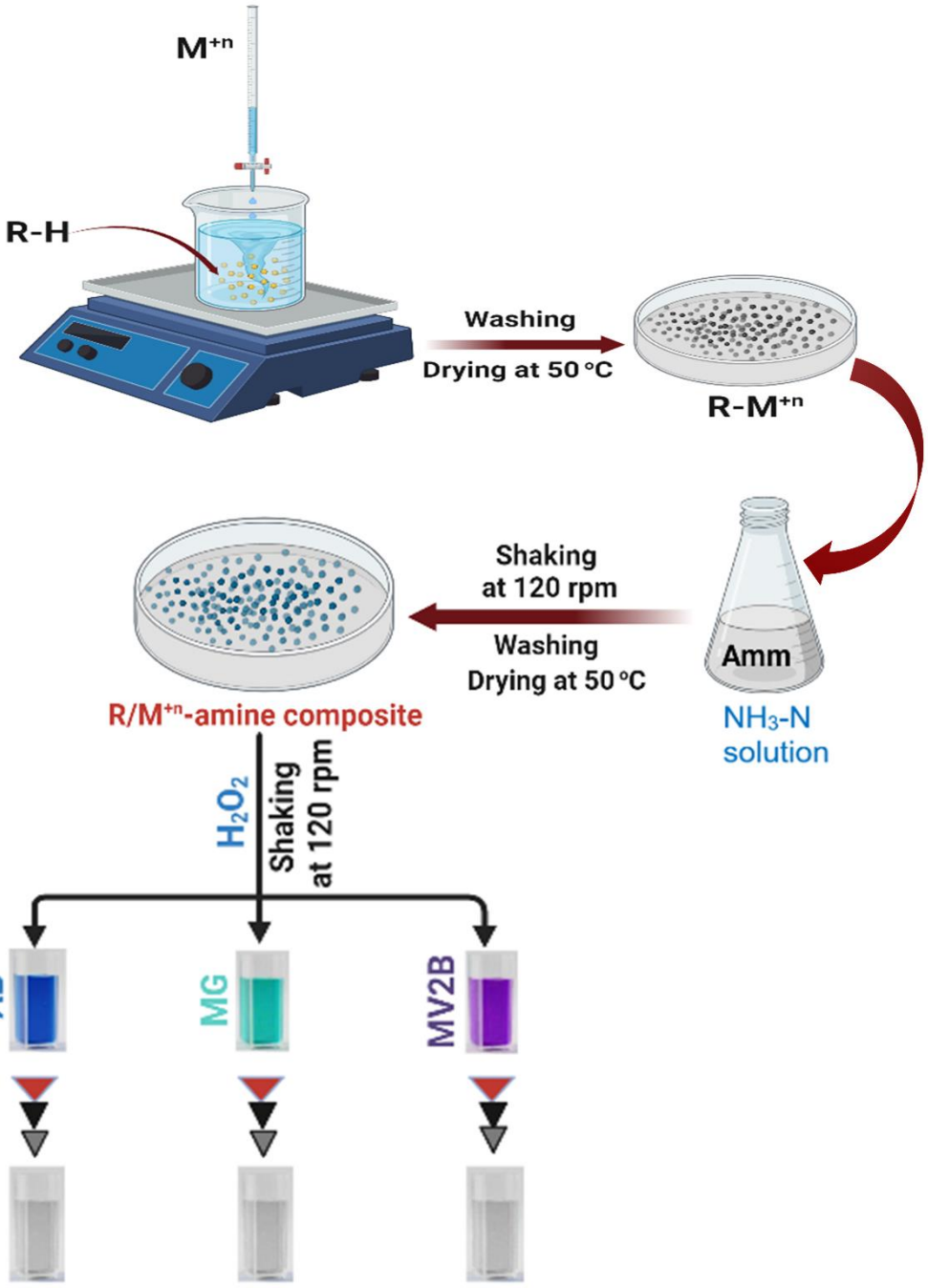

708

709

Figures

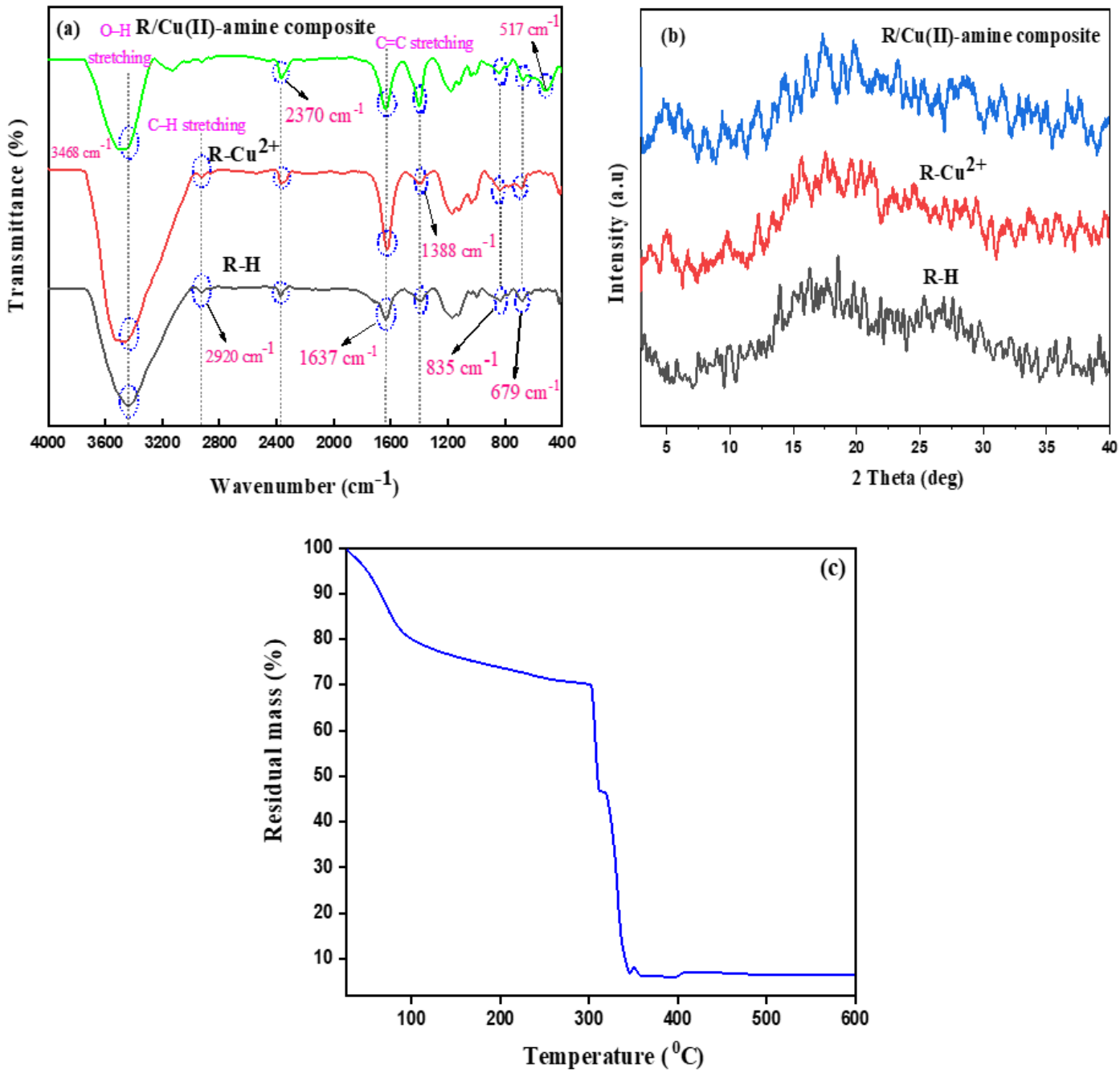

Figure 1

(a) FT-IR spectra of R-H, R-Cu^{2+}, and R/Cu(II)-amine composite; (b) XRD patterns of R-H, R-Cu^{2+}, and R/Cu(II)-amine composite; (c) TGA curve of R/Cu(II)-amine composite.

Figure 2

(a) SEM images of R-H; (b) SEM images of R-Cu^{2+}; (c) SEM images of

R/Cu(II)-amine composite; (d) EDX image of R/Cu(II)-amine composite.

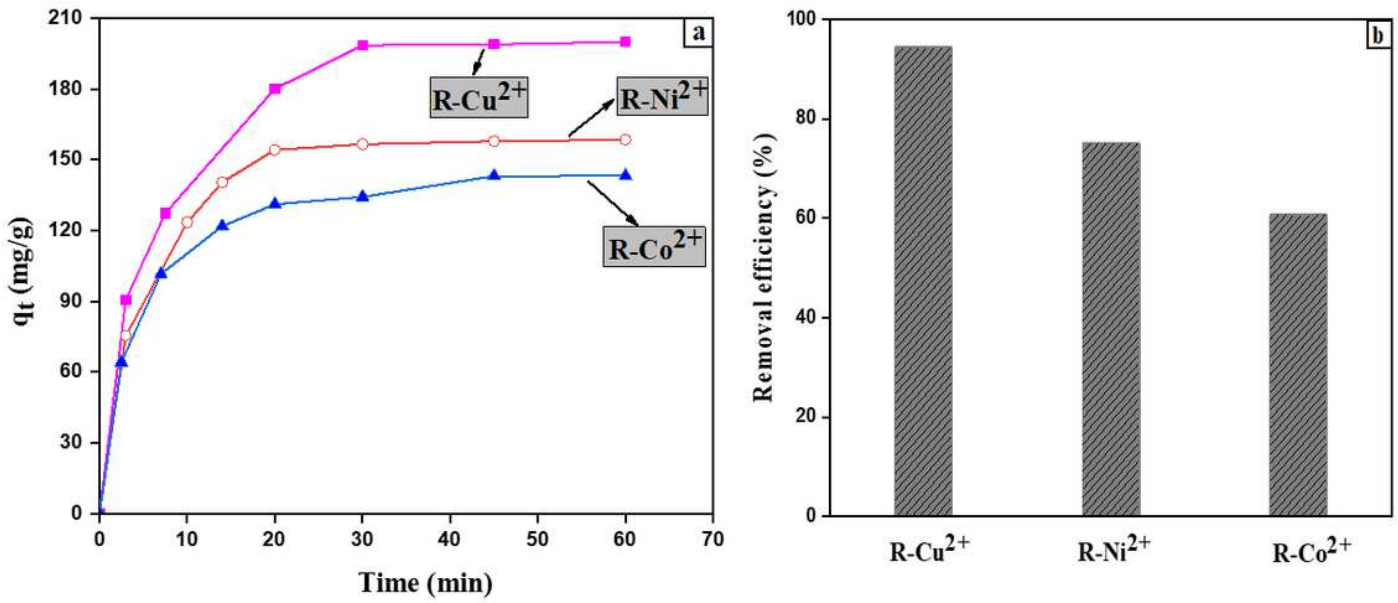

Figure 3

(a) Effect of contact time on the adsorption capacities of NH_4^+; (b) The removal efficiency of NH_4^+ onto R-Cu^{2+}, R-Ni^{2+} and R-Co^{2+} (0.1 g) using $[NH_4^+]_o$ =1060 mg. L^{-1}, 130 rpm and 30 ^oC.

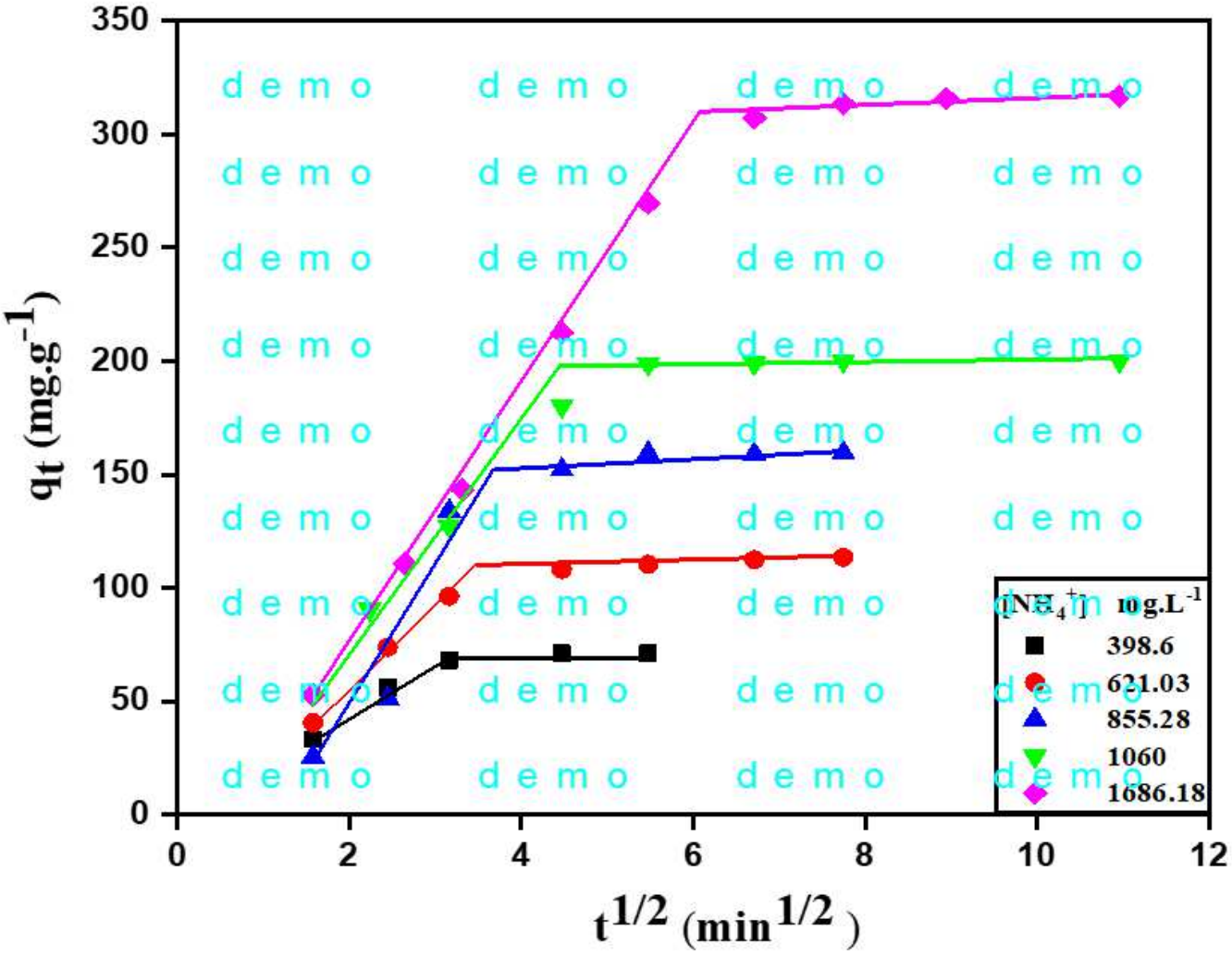

Figure 4

Intra-particle diffusion plot of the adsorption of NH_4^+ onto (0.1 g) of R-Cu^{+2} at 30 ^oC.

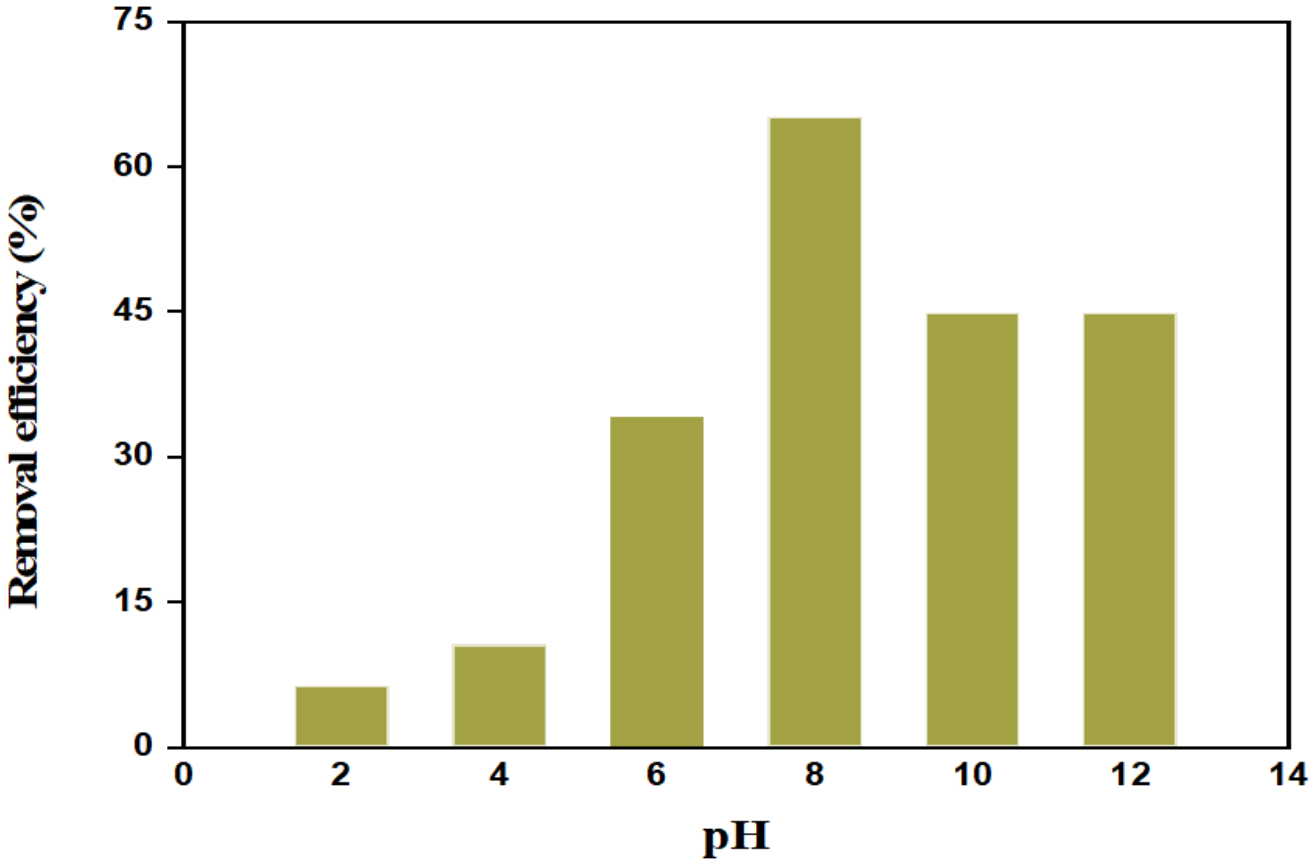

Figure 5

The effect of initial pH on the removal efficiency of NH_3-N, $[NH4^+]_o$ = 1032.9 mg. L^{-1} using R-Cu^{2+} (0.1 g) at 30 ^oC.

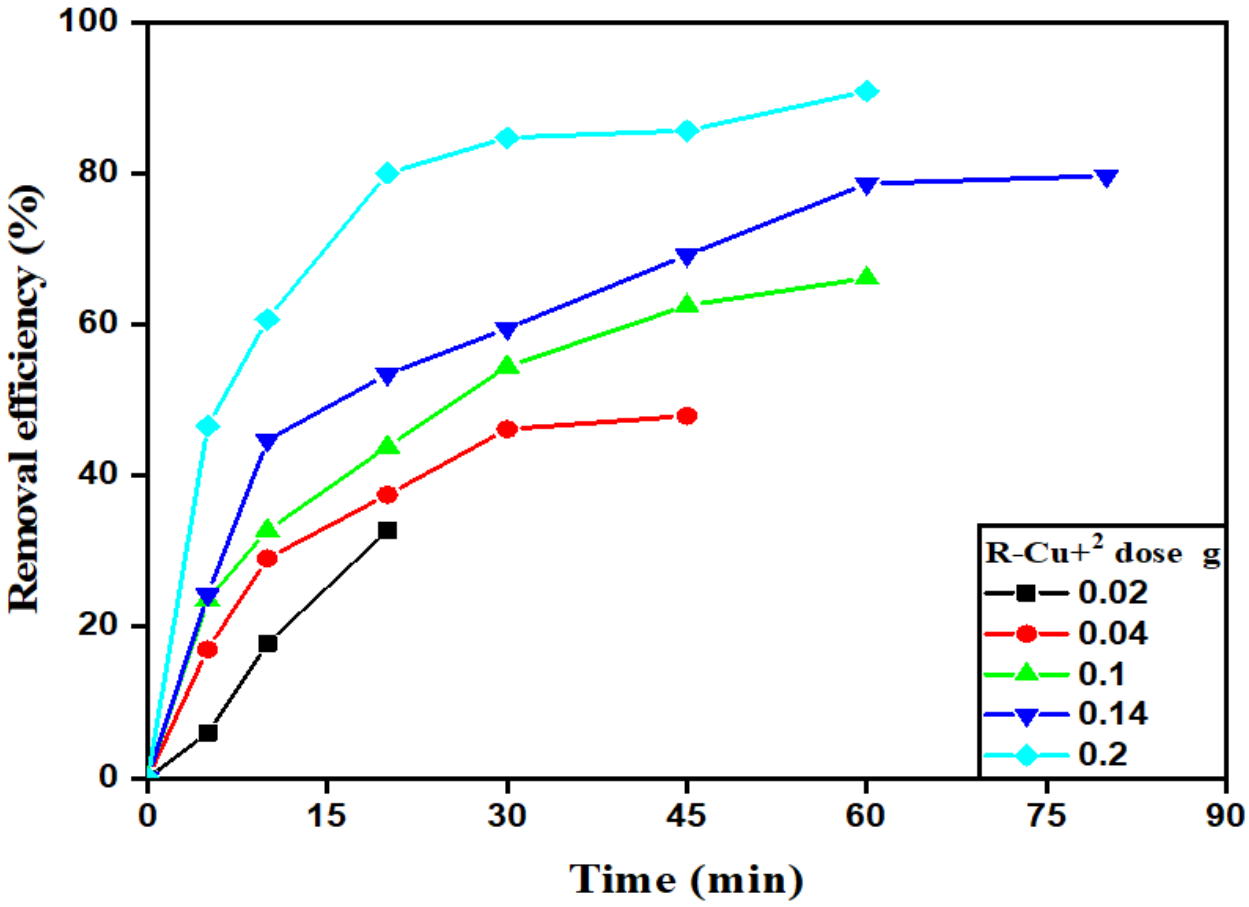

Figure 6

The effect of dose (R-Cu^{2+}) on the removal efficiency of NH_3-N, $[NH4^+]_o$ = 1032.9 mg. L^{-1}, pH = 8.6 and temperature 30 ^oC.

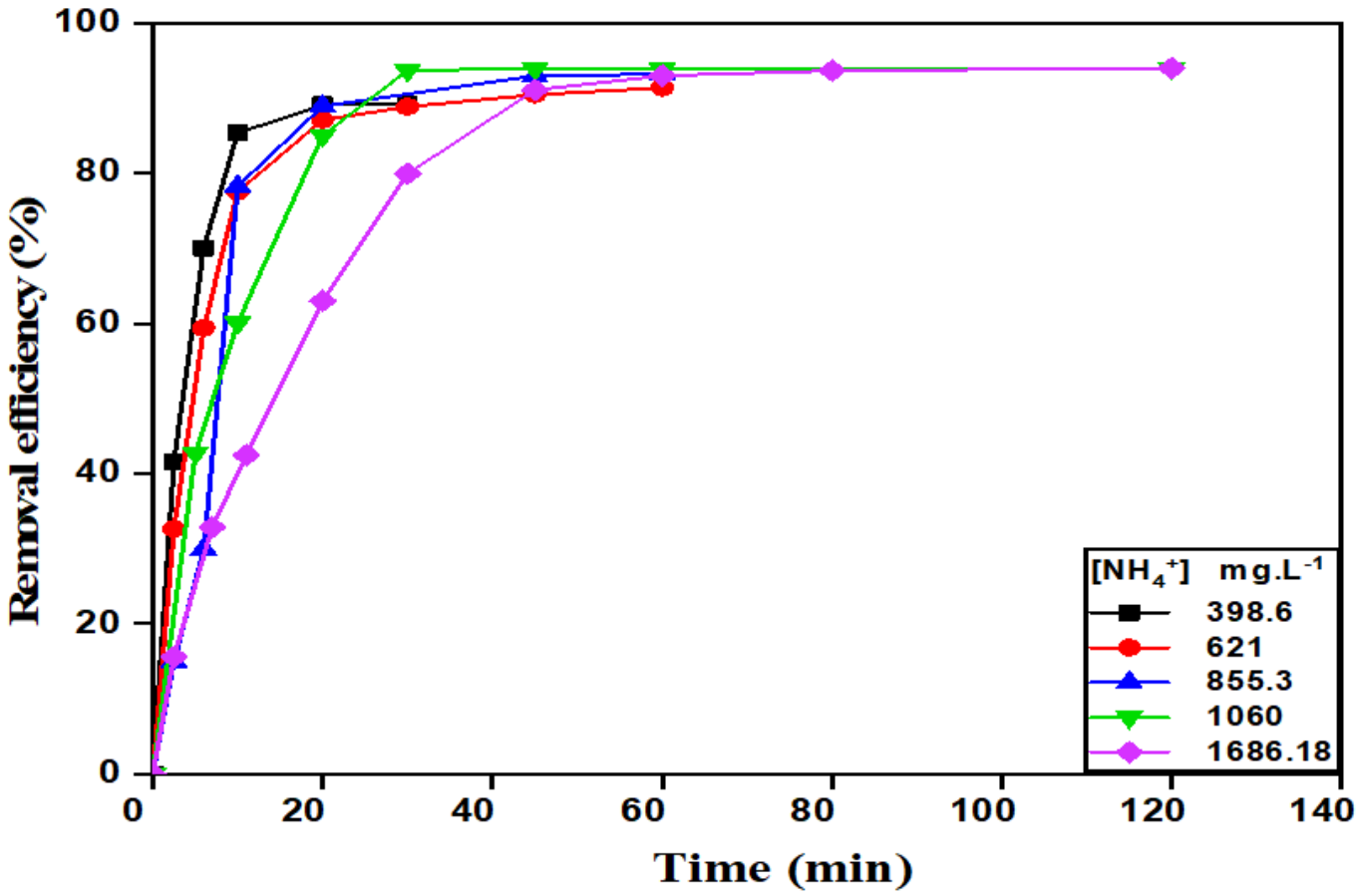

Figure 7

Influence of initial concentration of NH_3-N solution on the removal efficiency at different time using R-Cu^{2+}= 0.1 g, pH= 8.6 at 30 ^oC.

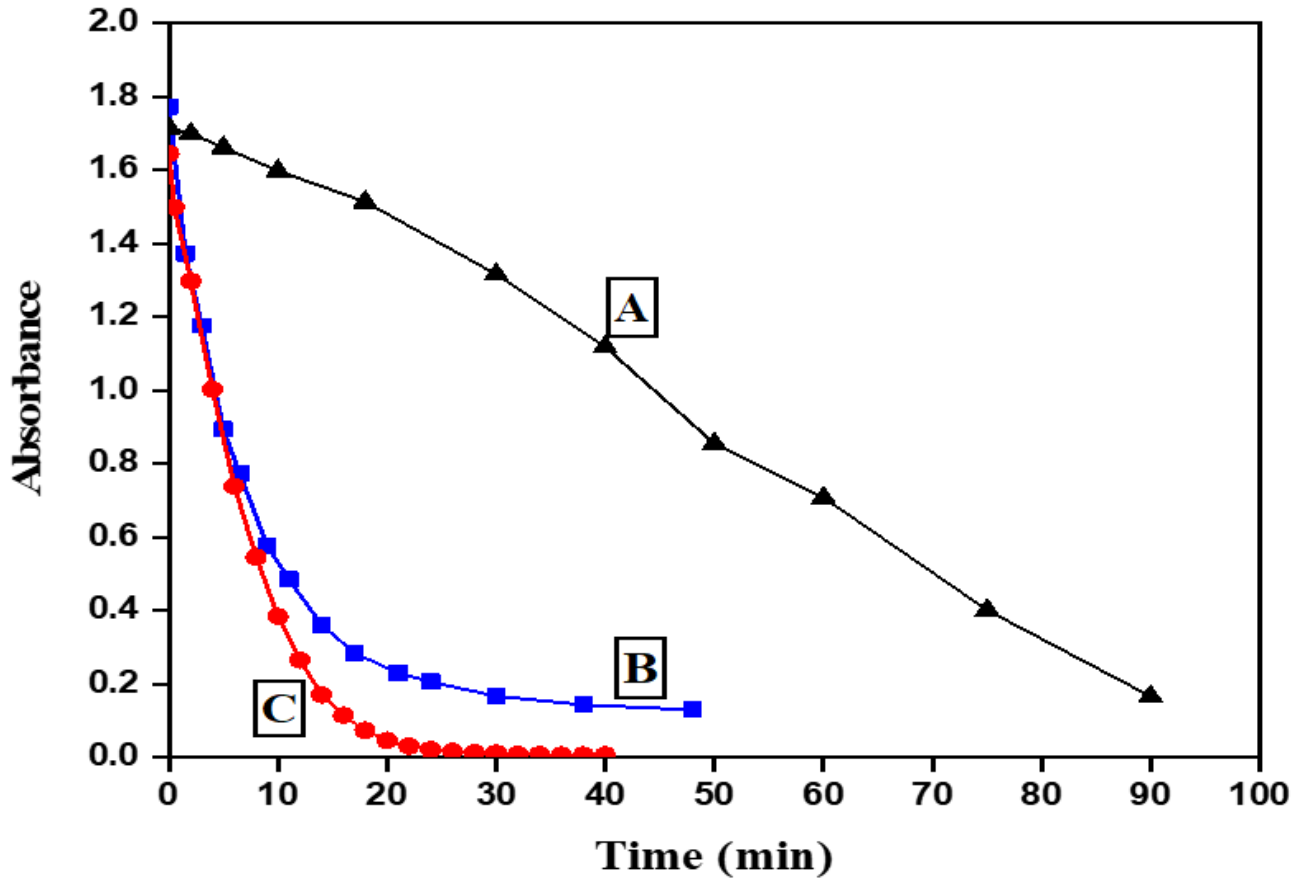

Figure 8

Absorbance-time plots for the catalytic degradation of different types of organic dyes using 0.05 g of R/Cu(II)-amine composite as a catalyst in the presence of $[H_2O_2]$ = 0.01 mol L^{-1} at 30 °C: **(A)** [MV] = 1.86 x 10^{-4} mol L^{-1}, **(B)** [AB]= 7.5 x 10^{-5} mol L^{-1}, and **(C)** [MG]= 2.5 x 10^{-5} mol L^{-1}.